



OPEN A V-band high-gain gap waveguide-based slot array antenna with circular polarization

Ali Sabbaghi Saber^{1,2}✉, Mohammad Soleimani² & Davood Zarifi^{1,3}

A high-gain circularly polarized (CP) slot array antenna is developed in the current work, based on ridge gap waveguide (RGW) technology for V-band applications. This antenna operates in the unlicensed 60-GHz band, which is designed for high-data-rate wireless communication systems. An asymmetric T-shaped slot is utilized in this design as the radiating element, ensuring compactness and lessening grating lobes. The array's structure features a 16×16 planar configuration and a corporate feed network. As shown by experimental and simulated results, there is a 3-dB axial ratio (AR) bandwidth and an impedance bandwidth of 6.6% spanning the frequency range of 58 to 62 GHz. Thus, an efficiency of up to 90% and a peak gain of 29.2 dBi is achieved. The performance of the manufactured antenna, encompassing gain, radiation patterns, and reflection coefficient, has been verified, indicating strong consistency with the simulation results. This design is well-suited for mmWave applications, which require a compact structure, circular polarization, and high gain.

The recent increase in the saturation of the spectrum at microwave frequencies has drawn renewed interest in millimeter waves. Therefore, the unlicensed 60-GHz frequency band (between 57 and 66 GHz) is competent for high data rate wireless communications¹⁻². Nevertheless, the high propagation path loss and strong oxygen absorption significantly affect the development of millimeter wave technology in this band. Hence, the antenna is a crucial component for most mmWave applications, requiring the ability to provide high radiation efficiency, a wide bandwidth, and high gain features. A survey is conducted on the 60-GHz band using arrays that present a gain above 30 dBi, which can be utilized for communication distances exceeding 100 m³. Moreover, planar antennas are highly sought after due to the need for compact system designs.

Furthermore, compared to linearly polarized antennas, CP antennas offer several advantages, including flexibility in orientation between receiving and transmitting antennas, as well as suppression of multipath interference⁴. Thus, researchers have suggested a large number of mmWave CP antennas for mmWave applications, including point-to-point moving links, mmWave satellite communication, and other urban applications to remove unmatched polarization and multipath interferences. Moreover, as demonstrated by investigations on propagation at the 60-GHz band, the wave with CP can offer enhanced channel performance compared to the linearly polarized wave⁵⁻⁶. Hence, it was found that the CP high-gain array antenna is a preferred case for the 60-GHz band.

CP array antennas can be designed in two ways. In the first approach, constituents with CP radiation are employed, which are fed into the array in phase and with the same amplitude. Here, the array's axial ratio (AR) bandwidth is equal to the element's AR bandwidth in the best case. Different elements are employed in the manufacturing of a CP array antenna, including a U-shaped slot patch⁷, a truncated microstrip patch⁸, a slot-fed rotated dipole antenna⁹, a magneto-electric dipole antenna¹⁰, a helical antenna¹¹, and an elliptical dielectric resonant antenna¹². In the second approach, sequential feeding is utilized. The sequentially rotating phase (SRP) feed is a widely used approach in designing a CP antenna array, employed to enhance polarization purity and bandwidth¹³. Nevertheless, SRP feeding approaches that rely on waveguide structures typically require a large area, creating challenges for array arrangement¹⁴⁻¹⁶. Alternatively, it is possible to achieve CP radiation by utilizing polarizers to transform the linear polarization (LP) beam into a CP beam¹⁷.

Based on the technology employed, CP array antennas can be categorized into two types: PCB-based antenna arrays and all-metal antenna arrays. First, substrate-based CP array antennas, like substrate-integrated waveguide (SIW)¹⁸ and low-temperature cofired ceramic (LTCC) technology¹⁹, are extensively used. The CP

¹School of Electrical and Computer Engineering, University of Kashan, Kashan, Iran. ²School of Electrical Engineering, Iran University of Science and Technology, Tehran, Iran. ³Department of Microwave and Antenna Engineering Faculty of Electronics, Telecommunications, and Informatics, Gdańsk University of Technology, 80-233 Gdańsk, Poland. ✉email: ali.sabbaghisaber@gmail.com

array antennas based on PCB are lightweight, compact, easy to manufacture, and compatible with different active and passive microwave structures. The low-power handling, leakage wave propagation at high frequencies, and high dielectric loss are the main factors that limit their functioning. Second, metal-based CP array antennas are excellent choices since there is no need to consider dielectric loss. Nevertheless, metal planar waveguide-based CP array antennas^{20–16} require a precision machining process to obtain an acceptable conductive connection between antenna layers, resulting in high manufacturing costs. Gap waveguide (GW) technology has been proposed for addressing the challenge of achieving good electrical contact in mechanical assembly²¹. In recent years, several CP array antennas utilizing GW technology have been proposed^{22–31}. These proposed antennas have relatively complex structures. Hence, there is a costly and complicated manufacturing process for these antennas.

A CP T-shaped slot linear array antenna has been recently presented based on groove gap waveguide (GGW) technology for Ka-band applications^{32,33}. In recent years, numerous studies have explored the impact of radiation slot geometries on antenna polarization characteristics. Structures incorporating orthogonal slots, U-shaped, and T-shaped slots have been widely used to achieve dual- or circular-polarization functionalities^{14,34–36}. The proposed array in³³ is a 1×10 linear array exhibits a 3-dB AR bandwidth of 8% from 28.9 to 31.3 GHz, an impedance bandwidth of 4% that covers 29.4 to 30.6 GHz, and 16.8 dBic as peak gain. The CP radiating element employed in this all-metal linear array is less complex than previous similar works, making the fabrication process cheaper and simpler. One such design features a 1×10 linear array, achieving a 4%, and a peak gain of 16.8 dBic. However, the principal limitation of this design lies in its inability to scale from a linear array to a planar configuration. This presents a considerable engineering challenge. It is widely recognized that 2D array antennas outperform 1D or linear slot arrays in terms of functionality and adaptability across advanced applications. Their standout feature is the ability to achieve full two-dimensional beam steering, which enables highly accurate target tracking, improved spatial resolution, and minimized signal interference—crucial for systems such as radar, satellite communications, and modern wireless networks. Moreover, 2D arrays deliver broader angular coverage and enable rapid adaptive beamforming, greatly enhancing system responsiveness and overall reliability.

The aforementioned challenge arises because, when assembling multiple GGW structures with sidewall pins to form a 2D array, the spacing between adjacent radiating slots exceeds $1\lambda_0$, thereby resulting in undesirable grating lobes in the radiation pattern. To overcome this issue, the feed network for the radiating slots must utilize E-plane groove gap waveguides or, more effectively, ridge gap waveguides. For optimal excitation, a ridge gap waveguide-based feed network is preferred. In this context, our proposed design exhibits several key differences compared to the configuration presented in³³. First, the ridge gap waveguide supports a distinct propagation mode, leading to substantial variations in antenna design methodology. Second, to realize effective excitation in a planar 2D array, we implement center-fed ridge gap waveguides, which help achieve radiation patterns with minimal beam squint. Third, the transition from ridge gap waveguide to standard rectangular waveguide in our design differs fundamentally from the approach described in³³, further underscoring the originality of our proposed structure.

In the present study, a CP 16×16 array antenna is proposed that employs asymmetric T-shaped slots as radiating elements for 60-GHz band applications. For preventing the grating lobe challenge in this structure, ridge gap waveguide (RGW) technology is used rather than GGW since it is more compact and has only one row of pins between adjacent ridges. This work is organized as follows: firstly, we shortly present and analyze the CP radiating element and a linear slot array. Then, the presented planar slot array antenna is designed and manufactured. Lastly, we present the measurement and simulation results and they are compared with reference works, which are presented as a table.

CP linear slot array antenna

The structure of a CP linear T-shaped slot array antenna is shown in Fig. 1, which consists of three major layers: the feeding layer, the waveguide layer, and the radiation layer. In the waveguide layer, a side-fed RGW receives energy via a coupling slot connected to the RGW feeding line at the bottom. The RGW feeding line is terminated by a PMC wall created using two rows of pins. Two steps are present at the beginning and end of the ridge in the waveguide layer to enhance matching and form a short-circuited section, respectively. The radiation layer consists of eight asymmetric T-shaped slots. The radiating element features two perpendicular arms: the first arm (active slot) is directly fed by the RGW line. In contrast, the second arm (parasitic element) is coupled to the active slot. A shift of s is introduced between the central axis of the parasitic element and the active slot, making the radiating element an asymmetric T-shaped slot. Moreover, a step with dimensions $b_3 \times h_3$ is added at the end of the parasitic element to enhance matching.

The radiating element demonstrated in Fig. 1 is used for producing right-handed CP (RHCP). For producing left-handed circular polarization (LHCP), the parasitic element's position should be mirrored relative to the center axis of the active slot. The symmetric T-shaped slot ($s=0$) can be utilized for creating linear polarization (LP) radiation.

The feed layer includes a ridge enclosed by a texture of pins so that the wave is only confined to the ridge (RGW). The pin dimensions must be selected to form a stop-band that spans the desired frequency range. For covering the entire unlicensed 60-GHz frequency band (57–66 GHz), the height, size, and periodicity of the pins, along with the air gap in our design, are specified as 1.5 mm, 0.75 mm, 1.75 mm, and 0.05 mm (zero-gap), respectively. Figure 2 presents the dispersion properties of the periodic pin arrangement. By optimizing these dimensions, optimal impedance matching and suitable radiation characteristics can be achieved.

To achieve a wide AR < 3 bandwidth and low reflection at the antenna input port, it is necessary to optimize the antenna parameters. The CST Microwave Studio is employed to optimize the antenna, and Table 1 lists the final values of the design parameters. Figure 3 presents the simulated results for $|S_{11}|$ and radiation features of

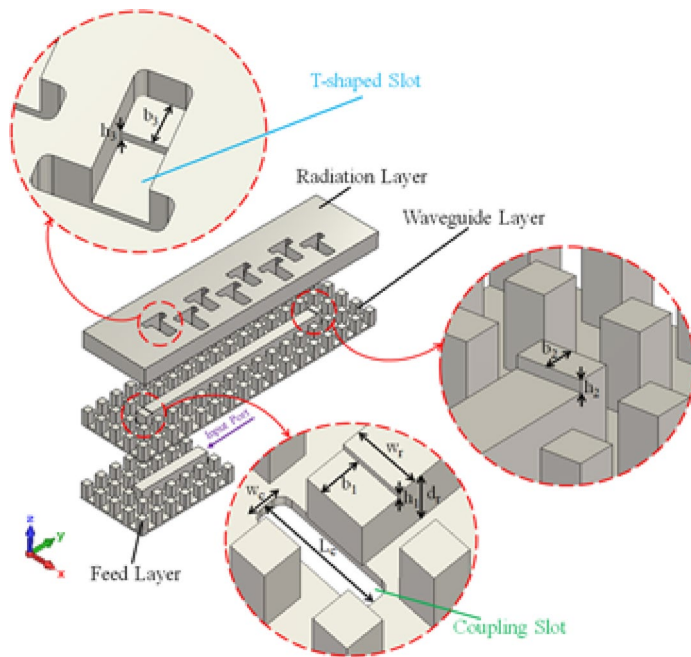


Fig. 1. Exploded perspective view of the layers of CP linear T-shaped slot array antenna.

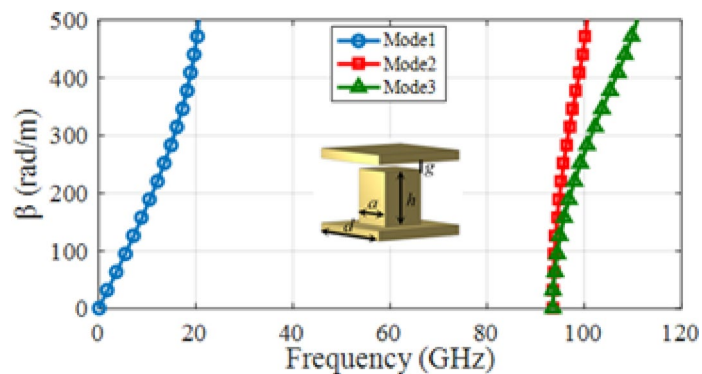


Fig. 2. Unitcell of periodic pin structure and its dispersion diagram for the first three modes. The design parameters are (in mm): $g=0.05$ mm, $a=0.75$ mm, $d=1.75$ mm, and $h=1.5$ mm.

Section	Parameter	Value (mm)
Active slot	Length	2.66
	Width	0.75
	Offset	0.70
	Spacing	2.70
Parasitic element	Length	2.27
	Width	1.14
	Depth	1.54
	s	0.20
	$b_3 \times h_3$	0.90 \times 0.37
Coupling slot	L_c	2.38
	w_c	0.65
Ridge	w_r	1.21
	d_r	1.28
	$b_1 \times h_1$	0.76 \times 0.15
	$b_2 \times h_2$	0.60 \times 0.23

Table 1. Design parameters of the CP linear slot array antenna.

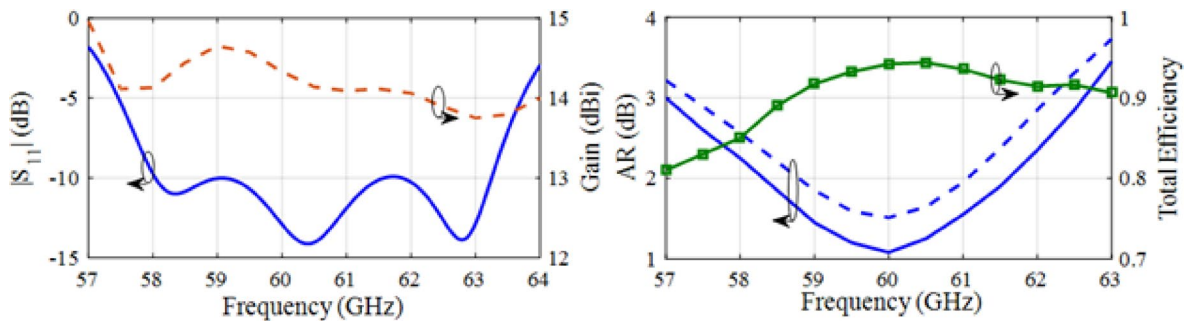


Fig. 3. Characteristics of CP linear slot array antenna. (a) $|S_{11}|$ and gain. (b) AR and total efficiency.

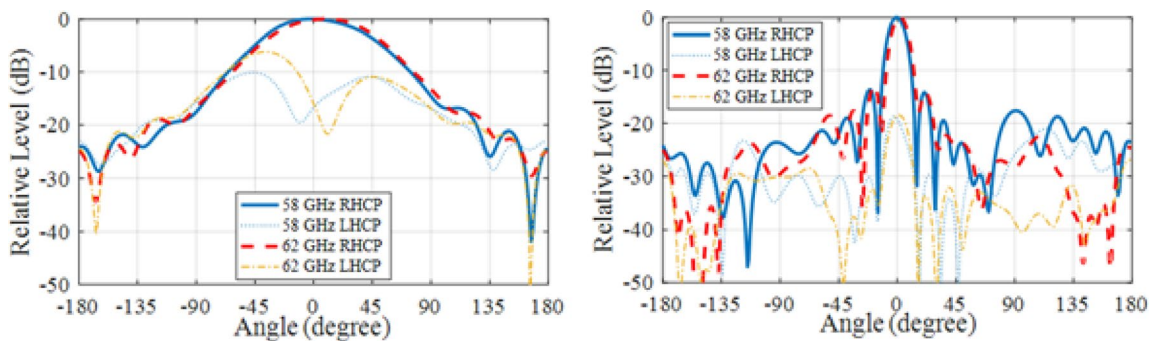


Fig. 4. Simulated normalized radiation patterns of the CP linear slot array antenna at frequencies 58 and 62 GHz. (a) xoz and (b) yoz planes.

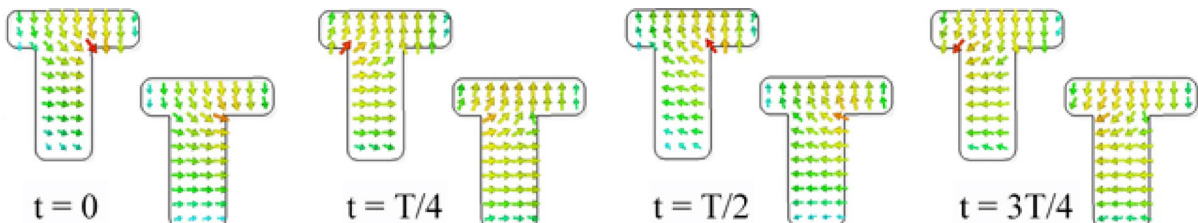


Fig. 5. Electric field distribution of the two adjacent radiating T-shaped apertures at 60 GHz.

the developed CP linear slot array antenna. The antenna has $|S_{11}| < -10$ dB, AR < 3 dB, efficiency above 83% from 58 to 62 GHz, and a peak gain of 14.6 dBic. Figure 3b shows the antenna's AR without a step placed at the end of the parasitic element with dashed lines. It is observed that the existence of this step has enhanced the axial ratio. Figure 4 indicates the normalized LHCP and RHCP radiation patterns of the antenna at two different frequencies in two orthogonal planes. It is noted that the cross-polarization level is smaller than -18 dB in both principal planes. Figure 5 shows the electric field distribution of the two neighboring radiating T-shaped apertures at 60 GHz. It describes the rotation of the electric field and the creation of CP radiation. To evaluate the impact of the parasitic element on the axial ratio of the CP antenna, parametric sweeps are conducted for the length and depth of the parasitic element, with the simulation results illustrated in Fig. 6. These results demonstrate that the parasitic element has a substantial effect on the CP radiation.

CP planar slot array antenna

To extend the developed linear array to a planar configuration, a corporate feed network is required. Figure 7 shows that this feed network includes a 16-way RGW power divider to excite a 16×16 slot array antenna. The designed configuration is symmetric. Thus, the power divider is in-phase, with its output ports having equal power division and the same phase. The V-form parts and chamfered corners in the power divider should be optimized to fulfill the matching requirements over the needed bandwidth. The initial value of $\lambda_g/4$ can be considered for L_m (λ_g = the guided wavelength) since this section can be interpreted as a quarter-wavelength transformer. The developed structure can be driven by a conventional V-band rectangular waveguide (such as WR-15) through the bottom surface, facilitating the measurement process. Additionally, to feed the array

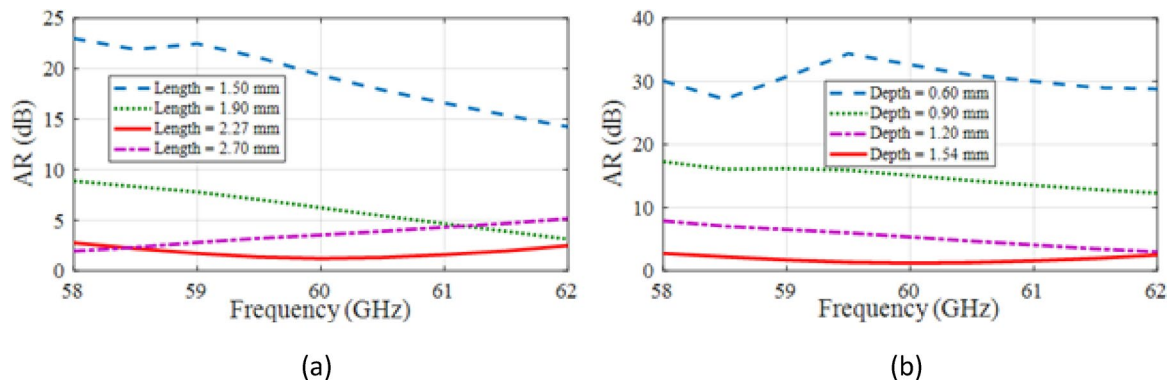


Fig. 6. The effect of the parasitic element (a) length (b) depth on the axial ratio of the CP linear slot array antenna.

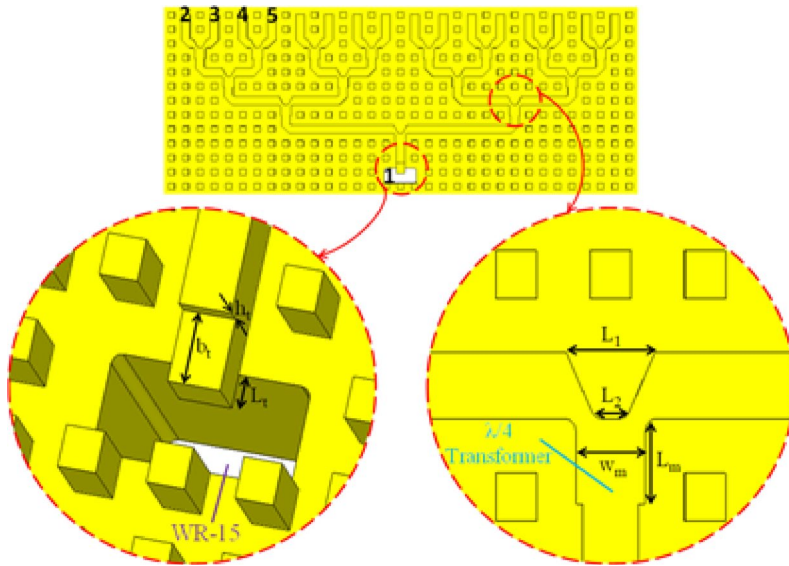


Fig. 7. The structure of the feed network for the excitation of a 16×16 slot array antenna. The top metal plate is not shown in the figure.

antenna via a conventional V-band flange, we created a simple transition from RGW to WR-15 ($3.9 \times 1.8 \text{ mm}^2$). Figure 7 shows the structural dimensions of the RGW to WR-15 transition. The transition's input matching is achieved through tuning the ridge's extended length to the waveguide opening (L_1) and the step dimensions ($b_1 \times h_1$). Figure 8 illustrates the simulated scattering parameters for the developed 16-way power divider. It shows that the input reflection coefficient is below -20 dB , while the amplitude imbalance is below $\pm 0.2 \text{ dB}$ in the needed frequency range from 58 to 62 GHz. To assess how the transition structure affects input matching, parametric sweeps are performed for the ridge extended length to the waveguide opening (L_1) and the step height (h_1), with the simulation results shown in Fig. 9. It can be seen that these parameters play a key role in achieving excellent matching at the input port of the transition.

The structure of the complete CP planar T-shaped slot array antenna is illustrated in Fig. 10a, where, in contrast to the linear antenna, the coupling slots are created at the center of the feeding ridges to overcome such obstacles as beam squint and narrow bandwidth. To obtain the required radiation and matching features across the specified bandwidth, we optimized the design parameters of radiation, feed layers, and waveguide. The optimized parameters for the planar slot array antenna are given in Table 2. The antenna size, including spaces for screws and alignment pins, is $78 \times 69 \times 10 \text{ mm}^3$.

Fabrication and measurement

Measurement results

A prototype of the CP 16×16 slot array antenna was manufactured from aluminum (electrical conductivity = $3.6 \times 10^7 \text{ S/m}$) using milling to confirm the performance of the developed array antenna. Some ineffective layer pins were replaced with metal blocks to decrease milling time. Figure 10b indicates the assembled

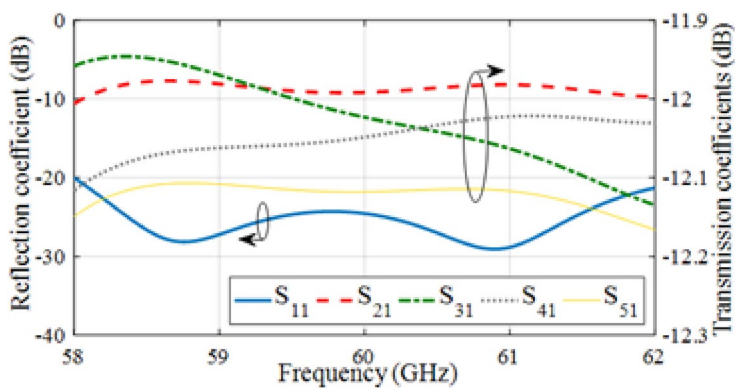


Fig. 8. Simulated S-parameters of 16-way ridge gap waveguide power divider.

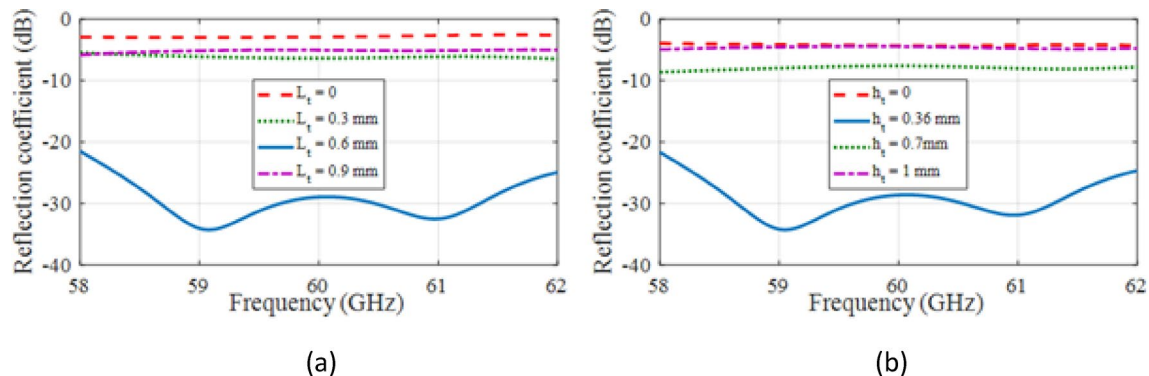


Fig. 9. Variation of simulated input reflection coefficient of 16-way ridge gap waveguide power divider for different values of (a) L_t , (b) h_t .

antenna, and Fig. 10c illustrates the antenna under test. Eight alignment pins and eight screws are used around the radiation aperture to ensure proper assembly of the antenna.

A vector network analyzer, linked to a WR-15 input interface, is used to measure the reflection coefficient of the antenna. Fig. 11a indicates the comparison between the measurement and simulation results for AR and the input reflection coefficient ($|S_{11}|$) of the antenna. The reflection coefficient of the antenna from 58 to 62 GHz is smaller than -10 dB, demonstrating an impedance bandwidth (IBW) of 6.6%. The 3-dB AR bandwidth of the antenna is 6.6% covering the range from 58 to 62 GHz. Moreover, Fig. 11b illustrates the antenna efficiency and boresight gain as a function of frequency. The antenna gain exceeds 29 dBi from 58 to 62 GHz, with a maximum gain of 29.2 dBi at 61 GHz. The antenna exhibits an efficiency of nearly 90% at 61 GHz, with an antenna gain of 29.2 dBi. It is possible to attribute the minor deviations between the simulated and measured results to misalignments between different layers, deviations in aluminum conductivity, measurement errors, and fabrication tolerances.

Figure 12 shows the simulation and measurement results for the normalized CP radiation patterns of the antenna. The highest side-lobe level of the antenna is approximately -13 dB in measurement and simulation. Moreover, the cross-polarization level is smaller than -18 dB.

Discussion

As summarized in Table 3, the proposed CP antenna array demonstrates a compelling balance of performance, efficiency, and structural simplicity compared to previously reported designs. Several prior works utilize SIW technology, achieving efficiencies below 72% while requiring three-layer structures. Although²⁰ achieves a notably high peak gain of 38.5 dBi and efficiency of 82%, it relies on a massive 32×32 array, which significantly increases design complexity and footprint. This work employs an RGW-based 16×16 array operating at 60 GHz, achieving a peak gain of 29.2 dBi, a peak efficiency of 90%, and a bandwidth of 6.6%, all within a three-layer structure. These specifications represent a significant advancement in high gain without excessive array scaling, exceptional efficiency, reasonable bandwidth, and moderate structural complexity, facilitating manufacturability. Moreover, the use of groove waveguide (GW) in both the antenna and feeding network layers contributes to low ohmic and dielectric losses, further enhancing overall performance. Given these advantages, the proposed CP antenna array stands out as a highly efficient, compact, and manufacturable solution for high-frequency applications, outperforming many existing designs in terms of both electrical and structural metrics.

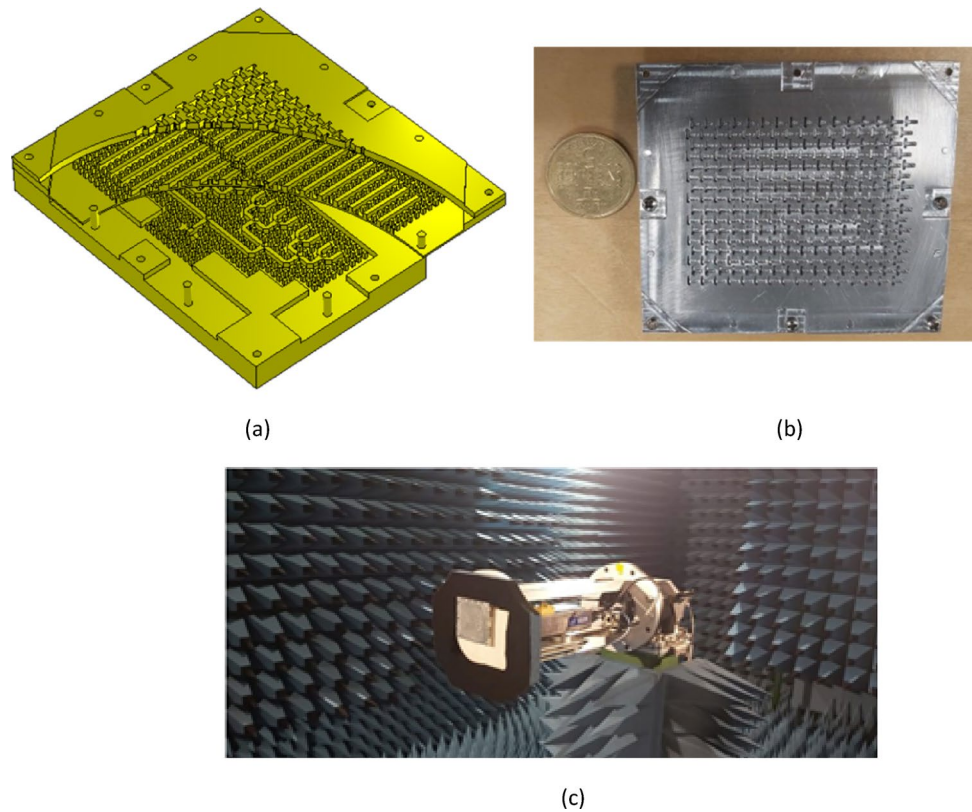


Fig. 10. (a) Configuration of CP planar slot array antenna. (b) photograph of assembled fabricated antenna. (c) photograph of under test antenna.

Section	Parameter	Value (mm)
Active slot	Length	2.60
	Width	0.73
	Offset	0.55
	Spacing	2.67
Parasitic element	Length	2.39
	Width	0.97
	Depth	1.58
	s	0.18
	$b_3 \times h_3$	0.85×0.32
Coupling slot	L_c	2.27
	w_c	0.80
Ridge	w_r	1.03
	d_r	1.39
	$b_1 \times h_1$	0.47×0.05
	$b_2 \times h_2$	0.47×0.10
Feed network	L_1	1.63
	L_2	0.69
	$L_m \times w_m$	1.33×1.26
	L_t	0.60
	$b_t \times h_t$	1.28×0.36

Table 2. Design parameters of the CP planar slot array antenna.

Conclusion

A 16×16 planar CP slot array antenna was designed and tested effectively using RGW technology, achieving efficient performance and high gain at the 60-GHz frequency band. By utilizing a corporate feed network and asymmetric T-shaped slots, grating lobes were minimized, resulting in high polarization purity and a compact structure. There was a close correlation between empirical measurements and simulations, verifying the antenna's capability to maintain a peak gain of 29.2 dBi with a 3-dB AR across the band, making it highly suitable for V-band wireless applications. The developed design integrates ease of fabrication, low loss, and exceptional performance, making it an excellent choice for high-frequency communication systems.

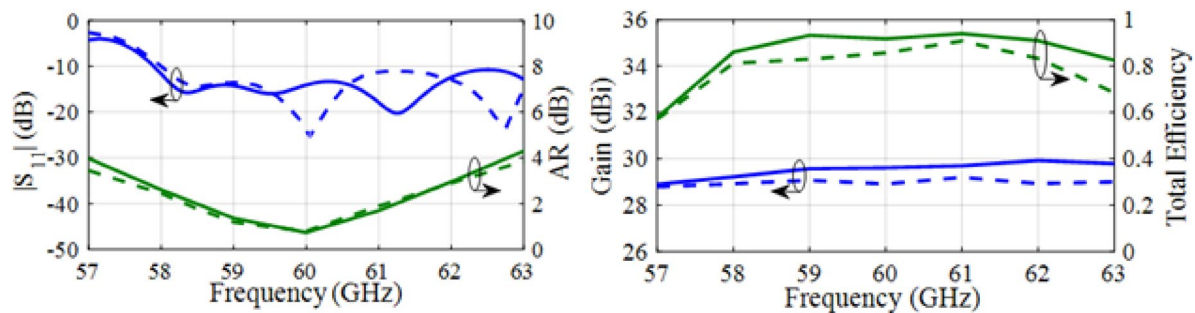


Fig. 11. Simulation and measurement results of proposed CP planar slot array antenna. **(a)** $|S_{11}|$ and AR. **(b)** Gain and efficiency. Measured values are shown with dashed-lines.

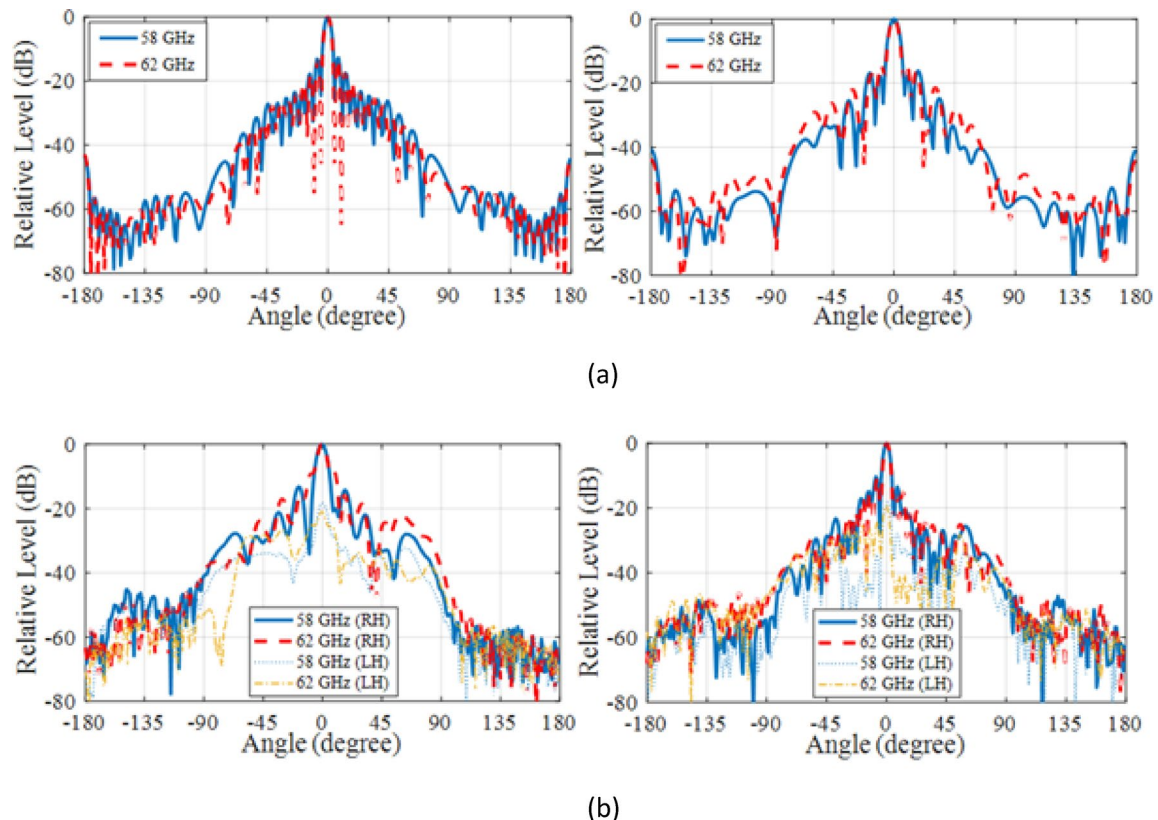


Fig. 12. Normalized radiation patterns of proposed CP planar slot array antenna in both principal planes. **(a)** Simulated. **(b)** Measured.

Ref	Technology	Array size	f_0 (GHz)	IBW (%)	ARBW (%)	Peak gain (dBic)	Peak efficiency (%)	No. of layers
9	SIW	4×4	60	28.1	19.2	16.7	52.5	3
10	SIW	8×8	60	18.2	16.5	26.1	72.2	3
14	Hollow waveguide	6×8	30	3	1	23.6	-	3
20	Hollow waveguide	32×32	61.5	15.8	15.1	38.5	82	6
23	RGW	1×8	78	6.5	6.5	14.8	84	2
30	RGW	8×18	77.5	3.9	3.9	27.3	85	2
31	RGW	1×8	77	3.9	3.2	15	78	4
34	GGW	1×10	30	4	8	16.5	98	2
This work:	RGW	16×16	60	6.6	6.6	29.2	90	3

Table 3. Comparison with other reported CP array antennas.**Data availability**

All data generated or analysed during this study are included in this published article.

Received: 26 April 2025; Accepted: 10 October 2025

Published online: 17 November 2025

References

1. Smulders, P. Exploiting the 60 GHz band for local wireless multimedia access: prospects and future directions. *IEEE Commun. Mag.* **40**(1), 140–147 (2002).
2. Rappaport, T. S., Murdock, J. N. & Gutierrez, F. State of the Art in 60-GHz Integrated Circuits and Systems for Wireless Communications, in Proceedings of the IEEE, vol. 99, no. 8, pp. 1390–1436. (2011).
3. Zhang, Y. P. & Liu, D. Antenna-on-Chip and Antenna-in-Package Solutions to Highly Integrated Millimeter-Wave Devices for Wireless Communications. *IEEE Trans. Antennas Propag.* **57**(10), 2830–2841 (2009).
4. C. A. Balanis, *Modern Antenna Handbook*. John Wiley & Sons, Incorporated, Google-Books-ID: Q9OgkQEACAAJ.
5. Manabe, T., Miura, Y. & Ihara, T. Effects of antenna directivity and polarization on indoor multipath propagation characteristics at 60 GHz. *IEEE J. Sel. Areas Commun.* **14**(3), 441–448 (1996).
6. Manabe, T. et al. Polarization dependence of multipath propagation and high-speed transmission characteristics of indoor millimeter-wave channel at 60 GHz. *IEEE Trans. Veh. Technol.* **44**(2), 268–274 (1995).
7. Sun, H., Guo, Y. X. & Wang, Z. 60-GHz circularly polarized U-slot patch antenna array on LTCC. *IEEE Trans. Antennas Propag.* **61**(1), 430–435 (2013).
8. Deng, C., Li, Y., Zhang, Z. & Feng, Z. Sequential-Phase Fed Circularly Polarized Patch Array. *IEEE Trans. Antennas Propag.* **62**(7), 3890–3893 (2014).
9. Li, Y. et al. Axial ratio bandwidth enhancement of 60-GHz substrate integrated waveguide-fed circularly polarized LTCC antenna array. *IEEE Trans. Antennas Propag.* **60**(10), 4619–4626 (2012).
10. Li, Y. & Luk, K. M. A 60-GHz Wideband Circularly Polarized Aperture-Coupled Magneto-Electric Dipole Antenna Array. *IEEE Trans. Antennas Propag.* **64**(4), 1325–1333 (2016).
11. Liu, C., Guo, Y. X., Bao, X. & Xiao, S. Q. 60-GHz LTCC Integrated Circularly Polarized Helical Antenna Array. *IEEE Trans. Antennas Propag.* **60**(3), 1329–1335 (2012).
12. Yang, S. S., Chair, R., Kishk, A. A., Lee, K. F. & Luk, K. M. Study on sequential feeding networks for subarrays of circularly polarized elliptical dielectric resonator antenna. *IEEE Trans. Antennas Propag.* **55**(2), 321–333 (2007).
13. Hall, P. S., Dahele, J. S. & James, J. R. Design principles of sequentially fed, wide bandwidth, circularly polarised microstrip antennas. *Proc. Inst. Elect. Eng. Microw. Antennas Propag.* **136**(5), 381–389 (1989).
14. Dimitrov, K. C. et al. Circularly polarized T-shaped slot waveguide array antenna for satellite communications. *IEEE Antennas Wirel. Propag. Lett.* **19**(2), 317–321 (2020).
15. Liu, Y. et al. Band broadband circularly polarized slot antenna based on L-shaped waveguide cavity. *IEEE Antennas Wirel. Propag. Lett.* **20**(9), 1606–1610 (2021).
16. Wang, H. et al. Circularly polarized waveguide aperture array antenna with a wide axial ratio bandwidth. *IEEE Antennas Wirel. Propag. Lett.* **21**(8), 1644–1648 (2022).
17. Ferrando-Rocher, M., Valero-Nogueira, A., Herranz-Herruzo, J. I. & Teniente, J. 60 GHz Single-Layer Slot-Array Antenna Fed by Groove Gap Waveguide, in IEEE Antennas and Wireless Propagation Letters. *IEEE Antennas Wirel. Propag. Lett.* **18**(5), 846–850 (2019).
18. Zhu, Q., Ng, K. B. & Chan, C. H. Printed Circularly Polarized Spiral Antenna Array for Millimeter-Wave Applications. *IEEE Trans. Antennas Propag.* **65**(2), 636–643 (2017).
19. Zhang, W. et al. Circularly-polarized array antenna-in-package in LTCC technology. *IEEE Trans. Antennas Propag.* **61**(12), 6228–6232 (2013).
20. Zhang, M., Yamamoto, T., Hirokawa, J. & Ando, M. A wideband circularly polarized corporate-fed waveguide aperture array in the 60 GHz band. *IEEE Antennas Wirel. Propag. Lett.* **20**(9), 1824–1828 (2021).
21. Kildal, P. S., Alfonso, E., Valero-Nogueira, A. & Rajo-Iglesias, E. Local metamaterial-based waveguides in gaps between parallel metal plates. *IEEE Antennas Wirel. Propag. Lett.* **8**, 84–87 (2009).
22. Zang, Z., Zaman, A. U. & Yang, J. Single Layer Dual Circularly Polarized Antenna Array Based on Ridge Gap Waveguide for 77 GHz Automotive Radar. *IEEE Trans. Antennas Propag.* **70**(7), 5977–5982 (2022).
23. Wu, K. et al. Wideband circularly polarized septum antenna array with ridge gap waveguide feeding network for wireless application. *IEEE Trans. Antennas Propag.* **70**(5), 3882–3887 (2022).
24. Ferrando-Rocher, M., Herranz-Herruzo, J. I., Valero-Nogueira, A. & Bernardo-Clemente, B. Single-layer sequential rotation network in gap waveguide for a wideband low-profile circularly polarized array antenna. *IEEE access* **10**, 62157–62163 (2022).
25. Liu, Z., Qi, S. S., Yu, Y. & Wu, W. W-band single-layer circularly-polarised antenna based on compact gap waveguide. *IET Microw. Antennas Propag.* **18**(8), 601–607 (2024).
26. Sun, L., Zaman, A. U., Yan, B. & Sheng, W. High-efficiency single-layer corporate-feed gap waveguide based circularly polarized antenna array with compact size. *AEU - Int. J. Electron. Commun.* **183**, 155341 (2024).

27. Ferrando-Rocher, M., Herranz-Herruzo, J. I., Valero-Nogueira, A. & Bernardo-Clemente, B. Switchable T-slot for dual-circularly-polarized slot-array antennas in Ka-band. *IEEE Antennas Wirel. Propag. Lett.* **20**(10), 1953–1957 (2021).
28. Zarifi, D. et al. Design of a dual-CP gap waveguide fed aperture array antenna. *IET Microw. Antennas Propag.* **17**(9), 723–730 (2023).
29. Zang, Z., Zaman, A. U. & Yang, J. Single-layer dual-circularly polarized series-fed gap waveguide-based slot array for a 77 GHz automotive radar. *IEEE Trans. Antennas Propag.* **71**(5), 3775–3784 (2023).
30. Zang, Z., Ren, Q., Uz Zaman, A. & Yang, J. 77 GHz Fully Polarimetric Antenna System With Compact Circularly Polarized Slots in Gap Waveguide for Automotive Radar. *IEEE Trans. Antennas Propag.* **72**(7), 5578–5588 (2024).
31. Alazemi, A. J. et al. A gap waveguide-fed dual-circularly polarized antenna array for K-band applicaions. *AEU Intern. J. Electron. Commun.* **170**, 154855 (2023).
32. Ferrando-Rocher, M., Herranz-Herruzo, J. I., Sánchez-Escuderos, D. & Valero-Nogueira, A. A Novel Circularly-Polarized T-shaped Slot Array Antenna in Ka-band, 2020 14th European Conference on Antennas and Propagation (EuCAP), Copenhagen, Denmark, pp. 1–3 (2020).
33. Herranz-Herruzo, J. I., Ferrando-Rocher, M., Valero-Nogueira, A. & Bernardo-Clemente, B. Novel asymmetric T-shaped radiating element for circularly-polarized waveguide slot arrays. *IEEE Trans. Antennas Propag.* **69**(11), 7452–7461 (2021).
34. Kyeong-Sik Min, J. et al. U-shaped slots for circularly polarized slotted waveguide array. *IEEE Antennas Propag. Soc. Intern. Symp.* **3**, 1434–1437. <https://doi.org/10.1109/APS.1995.530845> (1995).
35. Montisci, G., Musa, M. & Mazzarella, G. Waveguide slot antennas for circularly polarized radiated field. *IEEE Trans. Antennas Propag.* **52**(2), 619–623 (2004).
36. Jing, X., Zhu, Z., Wang, Y. & Peng, Y. Waveguide slotted array antenna for circularly polarized radiation field, *16th International Conference on Electronic Packaging Technology (ICEPT)*, Changsha, China, 2015, pp. 1398–1401, Changsha, China, 2015, pp. 1398–1401, <https://doi.org/10.1109/ICEPT.2015.7236841>(2015).

Author contributions

A. S. S. contributed to the conceptualization and design of the study and was involved in the drafting and revision of the manuscript. M. S. supervised the design and was involved in the drafting and revision of the manuscript. D. Z. contributed to the conceptualization and design of the study.

Declarations

Competing interests

The authors declare no competing interests.

Additional information

Supplementary Information The online version contains supplementary material available at <https://doi.org/10.1038/s41598-025-24159-5>.

Correspondence and requests for materials should be addressed to A.S.S.

Reprints and permissions information is available at www.nature.com/reprints.

Publisher's note Springer Nature remains neutral with regard to jurisdictional claims in published maps and institutional affiliations.

Open Access This article is licensed under a Creative Commons Attribution-NonCommercial-NoDerivatives 4.0 International License, which permits any non-commercial use, sharing, distribution and reproduction in any medium or format, as long as you give appropriate credit to the original author(s) and the source, provide a link to the Creative Commons licence, and indicate if you modified the licensed material. You do not have permission under this licence to share adapted material derived from this article or parts of it. The images or other third party material in this article are included in the article's Creative Commons licence, unless indicated otherwise in a credit line to the material. If material is not included in the article's Creative Commons licence and your intended use is not permitted by statutory regulation or exceeds the permitted use, you will need to obtain permission directly from the copyright holder. To view a copy of this licence, visit <http://creativecommons.org/licenses/by-nc-nd/4.0/>.

© The Author(s) 2025